First-principles method justifying the Dieke diagram and beyond

Katsuhiro Suzuki,[1] Takao Kotani,[2,3] and Kazunori Sato[1,3,4]

[1]*Division of Materials and Manufacturing Science, Graduate School of Engineering, Osaka University, Suita, Osaka 565-0871, Japan*
[2]*Advanced Mechanical and Electronic System Research Center (AMES), Faculty of Engineering, Tottori University, Tottori 680-8552, Japan*
[3]*CSRN-Osaka, Osaka University, Toyonaka, Osaka 560-8531, Japan*
[4]*Spintronics Research Network Division, OTRI, Osaka University, Toyonaka, Osaka 560-8531, Japan*

We present a method to determine the model Hamiltonians to treat rare-earth multiplets in solids from the results of the quasiparticle self-consistent *GW* (QSGW) method. We apply the method to trivalent Eu compounds $EuCl_3$, EuN, and Eu-doped GaN after examining free rare-earth ions. We solve the model Hamiltonian by the exact diagonalization. Our results justify applying the Dieke diagram to ions in solid, while its limitation is clarified. In particular, we show that the crystal fields cause sizable breaking of the Russell-Saunders coupling.

I. INTRODUCTION

The photoluminescence of rare-earth atoms (PLR) embedded in solids is one of the essential physical phenomena, which has a wide range of possible applications for light emitters. For example, Eu-doped GaN is a candidate for trichromatic LEDs, thanks to red-light emission by PLR of Eu [1–3]. It is favorable to assist the investigation of such PLR with the computations, that is, the computational materials design (CMD). However, CMD for PLR is not so easy because we do not have a reliable theoretical basis to perform computations for PLR even today.

Historically, the model-Hamiltonian methods based on the atomic multiplet theory had been developed to explain complex spectra of PLR, where the model Hamiltonian was parametrized by the Slater integrals [4], which are treated as material-dependent parameters. The atomic multiplet theory to determine the model Hamiltonian was given by Racah [5], followed by further developments [6–10]. Particularly, a comprehensive study by Dieke and Crosswhite on doubly and triply ionized rare earth (*RE*) is well known. The energy level diagram for all lanthanides in the study called the Dieke diagram is taken as a standard for analyzing experimental results even now [11]. The material-dependent parameters to give the Dieke diagram are determined experimentally so as to reproduce the optical spectra of PLR. Since we had no means to determine the parameters by computation, the model-Hamiltonian methods were quite limited from the view of CMD.

One of the recent theoretical approaches to treating the multiplets was given by Ungur and Chibotaru, who successfully applied the complete active space self-consistent-field method (CASSCF) [12] to lanthanide complexes [13,14].

However, applying CASSCF to handle *RE* in solids such as semiconductors should be difficult. This is because we have to consider the screening effects of the Coulomb interaction between $4f$ electrons caused by the polarization of host semiconductors. Furthermore, $4f$ orbitals can hybridize well with atomic orbitals in solids: the $4f$ orbitals can be itinerant or localized depending on their environments [15–18]. We have to use a method reproducing the properties of both *RE* and solids on the same footing. In CASSCF, it is hopeless from the view of high computational demand to use sufficiently large enough active space to reproduce the properties of solids. CASSCF is applicable to only the cases where $4f$ electrons are very localized.

We have other first-principles-based methods to handle the multiplets until now. Most of these methods have two key steps. One is how to determine the model Hamiltonian, and the other is how to solve the model, namely the solver. For the solver, we have extensive developments until now. Assuming the LDA+*U* model Hamiltonian, the Hubbard-I approximation [19,20] (HIA) and the dynamical mean-field theory (DMFT) have been developed to predict multiplet properties and peak structures of the excitation spectra [21–24].

A serious problem is in the first step. The reliability of widely used LDA+*U* is quite questionable. We usually have to give the size of *U* by hand. LDA+*U* assumes a very simple double-counting term. There are no parameters to control the center of $4f$ bands relative to the anion bands, that is, we simply assume that the center is determined in LDA. Considering these facts, we guess that LDA+*U* is often abused with little theoretical justifications as was analyzed by Lee, Kotani, and Ke [25]. Moreover, the multiplet excitation of *RE* is not controlled by *U* but by the 2nd Slater integral F_2 as we will explain later on.

In this paper, we will give a new method for the first step, deducing the parameters in the model Hamiltonian from the results of the quasiparticle self-consistent *GW* (QSGW) method [26]. QSGW is a reliable mean-field approximation in the sense that the one-particle Hamiltonian determined in QSGW gives a good independent-particle picture for a wide range of materials [26,27] including not only semiconductors

but also $4f$ systems [28]. QSGW is roughly identified to be a "screened" Hartree-Fock method where the screening effect is internally determined self-consistently. Both excitation energies and quantities such as spin fluctuations can be reproduced well based on the one-particle Hamiltonian in QSGW [29]. Let us explain our core idea about how to deduce the parameters in the model Hamiltonian. Our core idea is that we require "QSGW applied to the model Hamiltonian" should reproduce the (model part of) one-body Hamiltonian given in QSGW. In contrast to LDA, we have no theoretical problem applying QSGW to the model Hamiltonian.

In this paper, we apply our new method to the multiplets of $4f$ orbitals in RE compounds, $EuCl_3$, EuN, and Eu-doped GaN, after examining trivalent RE ions (RE^{3+}) in the supercell. The parameters of the model Hamiltonian for describing $4f$ electrons are obtained based on our core idea. With the exact diagonalization applied to the model Hamiltonian, we show the eigenvalues of multiplets of RE $4f$ orbitals and discuss the relation with experiments.

II. METHOD

We assume a model Hamiltonian of the multiplets with a fixed number of electrons of $4f$ orbitals. Here we neglect the hybridization of $4f$ orbitals with the other orbitals. Thus, the dimension of the model Hamiltonian is the number of the electronic configurations of $4f$ electrons, i.e., $_{14}C_n$ where n is the number of $4f$ electrons. Then, the model Hamiltonian is written as

$$\mathscr{H} = \mathscr{H}_0 + \mathscr{H}_{CF} + \mathscr{H}_{SOC} + \mathscr{H}_C. \tag{1}$$

$\mathscr{H}_0$ is a constant matrix to give the base level of $4f$. The level is irrelevant to energy spectra since we do not consider the hybridizations. The non-spherical part of the one-body potential is given by the crystal field term $\mathscr{H}_{CF}$. In addition, we have the spin-orbit coupling (SOC) term $\mathscr{H}_{SOC}$, and the effective Coulomb interaction term $\mathscr{H}_C$. Surrounding atoms of the RE atom affect not only $\mathscr{H}_{CF}$ but also $\mathscr{H}_C$ through the size of interaction, and $\mathscr{H}_{SOC}$ as well via the shape of $4f$ orbitals. $\mathscr{H}_{SOC}$ and $\mathscr{H}_C$ are given as

$$\mathscr{H}_{SOC} = \xi \sum_{\substack{mm' \\ \sigma\sigma'}} \left(l_x^{mm'} s_x^{\sigma\sigma'} + l_y^{mm'} s_y^{\sigma\sigma'} + l_z^{mm'} s_z^{\sigma\sigma'} \right) \hat{c}_{m\sigma}^\dagger \hat{c}_{m'\sigma'}, \tag{2}$$

$$\mathscr{H}_C = \frac{1}{2} \sum_{\substack{m_1,m_2, \\ m_3,m_4}} \sum_{\sigma\sigma'} g_{m_1m_2m_3m_4}^{\sigma\sigma'} \hat{c}_{m_1\sigma}^\dagger \hat{c}_{m_2\sigma'}^\dagger \hat{c}_{m_4\sigma'} \hat{c}_{m_3\sigma}. \tag{3}$$

Here indices $m, m', m_i (i = 1, 2, 3, 4)$ are for the magnetic quantum number, σ and σ' for spins, and $\hat{c}_{m\sigma}$ is the electron-annihilation operator. $\mathscr{H}_{SOC}$ is made of the strength of SOC ξ and the angular-momentum and spin matrices $l_x^{mm'}, s_x^{\sigma\sigma'}, \dots$. We assume the effective Coulomb interactions $g_{m_1m_2m_3m_4}^{\sigma\sigma'}$ are given as

$$g_{m_1m_2m_3m_4}^{\sigma\sigma'} = (-1)^{m_1-m_3} \delta_{m_1+m_2, m_3+m_4}$$
$$\times \sum_{p=0}^{l} F_{\sigma\sigma'}^{2p} c^{2p}(m_1, m_3) c^{2p}(m_2, m_4), \tag{4}$$

where we have the Gaunt coefficients $c^p(m, m')$ [30] and the Slater-Condon parameters $F_{\sigma\sigma'}^{2p}$ for $4f$ orbitals [4,31]. We use the scaled-Slater-Condon parameters F_0, ΔF_0, and F_2 to represent $F_{\sigma\sigma'}^{2p}$ as

$$\begin{cases} F_{\sigma\sigma'}^0 = F_0 + \delta_{\sigma\sigma'}\Delta F_0 \\ F_{\sigma\sigma'}^2 = 225F_2 \\ F_{\sigma\sigma'}^4 = 1089 \times 0.138F_2 \\ F_{\sigma\sigma'}^6 = 7361.64 \times 0.151F_2 \end{cases} \tag{5}$$

in the manner of Ref. [32] for analyzing the RE^{3+} elements. Here we fix the ratios $F_{\sigma\sigma'}^4/F_{\sigma\sigma'}^2$ and $F_{\sigma\sigma'}^6/F_{\sigma\sigma'}^2$ as in Ref. [33] respecting the case of hydrogen. The spin-dependent term $\delta_{\sigma\sigma'}\Delta F_0$ is introduced to make a compromise in our fitting procedure to the QSGW results with keeping the spin-space symmetry of the model Hamiltonian.

We assume a general crystal field that corresponds to the symmetry of each material. Using Steven's operators $(O_4^0)_{mm'}, (O_4^4)_{mm'}$, and so on [34], $\mathscr{H}_{CF}$ is given as

$$\mathscr{H}_{CF} = \sum_{\substack{mm' \\ \sigma\sigma'}} (h_{CF})_{mm'} \hat{c}_{m,\sigma}^\dagger c_{m',\sigma'} \tag{6}$$

$$h_{CF} = \begin{cases} B_4^0(O_4^0 + 5O_4^4) + B_6^0(O_6^0 - 21O_6^6) & \text{(cubic)} \\ B_2^0 O_2^0 + B_4^0 O_4^0 + B_6^0 O_6^0 + B_6^6 O_6^6 & \text{(hexagonal)} \end{cases}, \tag{7}$$

where $B_4^0, B_6^0, B_2^0, B_6^6$ are the parameters to specify crystal fields. Thus, the model Hamiltonian $\mathscr{H}$ of Eq. (1) is specified by parameters ξ, F_0, ΔF_0, F_2, and B_l^m.

To apply our core idea shown in the introduction, we should apply QSGW to the model Hamiltonian. Here we neglect the correlation part since we expect little screening effects of $4f$ orbitals by themselves. That is, we apply the Hartree-Fock approximation to $\mathscr{H}$ instead, resulting in the Hartree-Fock model Hamiltonian (HFMH) $\mathscr{H}_{HF}$ as

$$\mathscr{H}_{HF} = \mathscr{H}_0 + \mathscr{H}_{SOC} + \mathscr{H}_{CF} + \mathscr{H}_C^{HF},$$

$$\mathscr{H}_C^{HF} = \sum_{m_1,m_3} \sum_{\sigma} \left[\sum_{m_2,m_4} \left(g_{m_1m_2m_3m_4}^{\sigma\sigma} - g_{m_1m_2m_4m_3}^{\sigma\sigma} \right) \langle c_{m_2\sigma}^\dagger c_{m_4\sigma} \rangle \right.$$
$$\left. + g_{m_1m_2m_3m_4}^{\sigma\bar{\sigma}} \langle c_{m_2\bar{\sigma}}^\dagger c_{m_4\bar{\sigma}} \rangle \right] \hat{c}_{m_1\sigma}^\dagger \hat{c}_{m_3\sigma}, \tag{8}$$

where $\mathscr{H}_C^{HF}$ is the mean-field approximation to $\mathscr{H}_C$. $\bar{\sigma}$ denotes the opposite spin to σ, and $\langle \dots \rangle$ means the expectation values for the ground state. Based on our core idea, we compare $\mathscr{H}_{HF}$ with the $4f$ part of the one-body Hamiltonian $\mathcal{H}_{4f}^{QSGW}$ given in QSGW, so as to determine parameters in $\mathscr{H}$.

We use the ecalj package [35] to perform QSGW calculations. In practice, we use 20% LDA mixing (QSGW80) so as to reduce too-large exchange effects. We can take QSGW80 as a quick remedy to include the effects of the vertex correction, which enhances the screening effect by $\sim$20% [36,37]. In fact, QSGW80 can reproduce the experimental band gap very well [27,38]. We obtain $\mathcal{H}_{4f}^{QSGW}$ based on localized Wannier functions (it was implemented in ecalj) as $\langle w_m | \mathcal{H}_{4f}^{QSGW} | w_{m'} \rangle$. Here w_m and $w_{m'}$ are the Wannier functions generated by the one-shot projection of $4f$-type atomic-like seed orbitals [35,39].
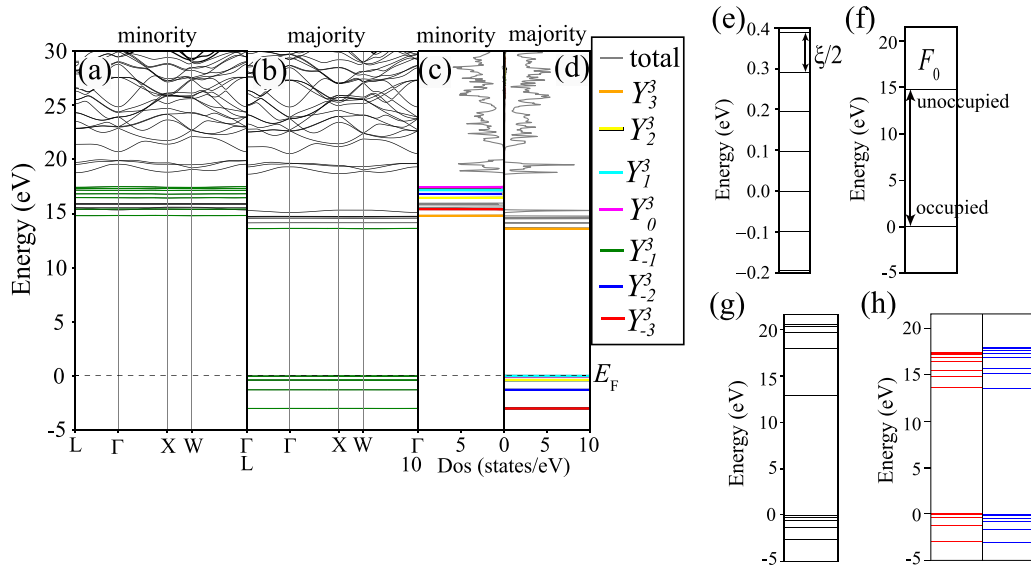
FIG. 1. [(a), (b)] Band structure of QSGW (black) and $\mathcal{H}_{4f}^{\text{QSGW}}$ (green) for free Eu^{3+} in a fcc supercell. [(c), (d)] DOS and PDOS corresponding to the QSGW band structure. (e)–(h) are for analyzing contributions of parameters $\xi, F_0, \Delta F_0$, and F_2 to $\mathcal{H}_{\text{HF}}$. We show eigenvalues (e) only with ξ; (f) only with F_0; and (g) only with F_0 and F_2. (h) Comparison of eigenvalues of $\mathcal{H}_{4f}^{\text{QSGW}}$ (red) and $\mathcal{H}_{\text{HF}}$ (blue). Spin-dependence is not resolved in (e)–(h).

In the QSGW calculations, we add the SOC term $\mathcal{H}_{\text{SOC}}^{\text{QSGW}}$ in the $L_z S_z$-only approximation. We obtain ξ by an average

$$\xi = \sqrt{\left(\sum_n \left| \langle w_n | \mathcal{H}_{\text{SOC}}^{\text{QSGW}} | w_n \rangle \right|^2 \right) \Big/ 14}. \tag{9}$$

Other parameters $F_0, \Delta F_0, F_2$, and B_l^m of $\mathcal{H}$ are determined to minimize the difference of eigenvalues between $\mathcal{H}_{4f}^{\text{QSGW}}$ and $\mathcal{H}_{\text{HF}}$. Then, we can obtain eigenvalues of $\mathcal{H}$ by the exact diagonalization [40].

In a summary, we mainly added two approximations to our core idea. One is $\mathcal{H}_{\text{HF}}$ instead of applying QSGW to the model Hamiltonian. The other is the QSGW80 instead of QSGW. In addition, we fix the ratios $F_{\sigma\sigma'}^4 / F_{\sigma\sigma'}^2$ and $F_{\sigma\sigma'}^6 / F_{\sigma\sigma'}^2$. We utilize the fixed ratio to enhance numerical stability and simple interpretation. In principle, our core idea is rather general for extracting an essential degree of freedom from the first-principles calculations. One of the advantages of our core idea is that we do not calculate effective interaction directly. The calculation of effective interaction is somehow complicated as discussed in Refs. [36,37], especially when we like to include vertex corrections.

III. RESULTS

Prior to discussion of the *RE* in compounds, we have examined free RE^{+3} in QSGW to confirm the performance of our method. For the calculation of the free RE^{+3}, we use a fcc supercell placing RE^{+3} at their centers, where RE^{+3} are separated by 7.07 Å. We assume a homogeneous background charge to keep charge neutrality.

In Figs. 1(a) and 1(b), we show the calculated band structure of Eu^{3+} in QSGW. We superpose that of $\mathcal{H}_{4f}^{\text{QSGW}}$ with green flat lines (seven lines per spin). PDOS of $4f$ orbitals is

shown in Figs. 1(c) and 1(d). Up to ∼18 eV, the calculated bands corresponding to $4f$, $5d$, and $6s$ are almost flat, indicating that our supercell is large enough. On the other hand, $6p$ bands around ∼20 eV have band width ∼1 eV because of the finite size of our supercell. The eigenvalue at Γ point around ∼21.5 eV is identified to be the vacuum level, the bottom of the scattering states. The band gap (LUMO-HOMO gap) is 13.7 eV, much larger than the LDA value of 4.85 eV. The majority bands of $4f$ orbitals except for $m = 3$ are occupied, that is, the ground state is $J_z = L_z + S_z = -3 + 3 = 0$, corresponding to $^7F_0$. Thus, our results are consistent with Hund's rule. Generally speaking, a good mean-field approach should

TABLE I. Parameters in eV determined in our method for free trivalent ions. The empirical studies in the right column correspond to the empirical values of Dieke's review paper [11]. These values are derived from many experimental and theoretical data [6,7,42–49].

|	Our method				Empirical study	
	F_0	ΔF_0	ξ	F_2	ξ	F_2
Pr	16.107	0.025	0.106	0.043	0.091 [47]	0.038 [47]
Nd	16.573	0.108	0.123	0.049	0.109	0.042
Pm	16.672	0.282	0.143	0.062	0.133 [48]	0.043 [48]
Sm	17.479	0.352	0.162	0.059	0.149	0.046 [6]
Eu	14.803	0.481	0.195	0.058	0.164 [7]	0.050 [7]
Gd	17.317	0.000	0.208	0.058	0.196	0.050
Tb	15.740	−0.274	0.236	0.055	0.211 [7]	0.054 [7]
Dy	16.867	0.000	0.265	0.068	0.236	0.052 [6]
Ho	16.817	0.000	0.296	0.071	0.268 [48]	0.056 [48]
Er	16.905	0.000	0.329	0.078	0.303 [49]	0.053 [49]
Tm	16.228	0.192	0.365	0.080	0.329	0.056
Yb	10.610	0.000	0.404	0.073	0.357	
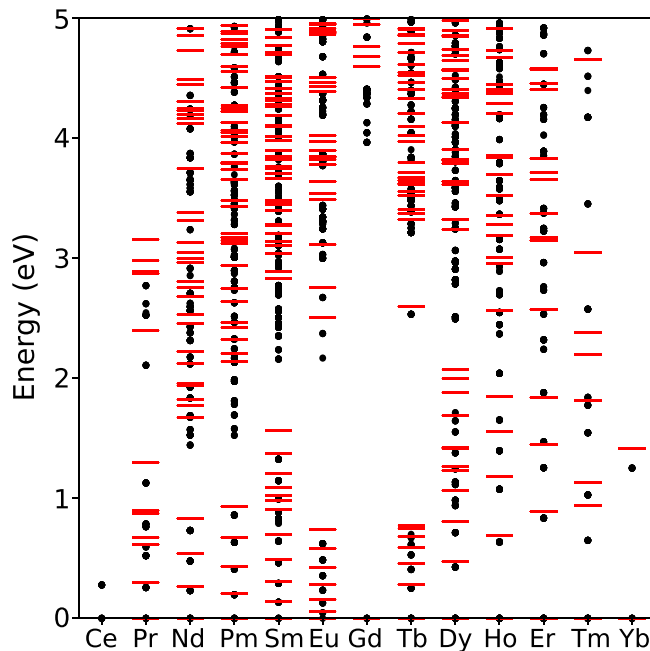
FIG. 2. Eigenvalues of *RE* ions. Dieke diagram is shown by the black points. Our results are superposed by red lines. Both are calculated from parameters in Table I.

satisfy Hund's rule since the ground states of atoms should be essentially described by the electronic configuration of a single Slater determinant.

We determine F_0, ΔF_0, and F_2 in $\mathcal{H}_{HF}$ so as to reproduce eigenvalues of $\mathcal{H}_{4f}^{QSGW}$. We see the eigenvalues match well as shown in Fig. 1(h). Figures 1(e)–1(h) show our analysis of how the parameters affect the eigenvalues of $\mathcal{H}_{HF}$. Figure 1(e) shows ξ splits into seven states with degeneracy between $m\sigma$ and $-m\bar{\sigma}$. Figure 1(f) shows that F_0 makes the difference between occupied and unoccupied states. Figure 1(g) shows that F_0 with F_2 is still not enough to reproduce $\mathcal{H}_{4f}^{QSGW}$. The parameter ΔF_0 is for describing larger effective interaction between occupied orbitals than that between occupied and unoccupied orbitals. This is reasonable because occupied $4f$ orbitals are localized more than unoccupied orbitals.

In Table I, we summarize obtained ξ, F_0, ΔF_0, and F_2 for RE^{+3} in our method. The QSGW results are in the Supplemental Material [41]. We skipped Ce since QSGW did not give localized $4f$ eigenfunctions. Table I shows that ξ and F_2 in our method give good agreements with those of empirical studies: their differences are only ∼10%. This is a justification for our method. F_0, corresponding to U of LDA+U, is changing systematically along the atomic number. Except for Gd, F_0 is the

largest in the middle of the first half and the latter half of the $4f$ series, namely at Sm when filling majority electrons, and at Er when minority. The latter half of the species shows a little larger values than the first half. F_2 systematically becomes larger along the atomic number. For example, the F_2 values of Tm and Pr are 0.080 eV and 0.043 eV, and the difference is 0.037 eV in our method, while the empirical study shows these F_2 values are 0.056 eV and 0.038 eV, and the difference is as 0.018 eV.

In Fig. 2, we compare the excitation energies of free RE^{3+} by the parameters of our method and by those of empirical studies in Table I. The latter exactly reproduced the original Dieke diagram [11]. In free RE^{3+}, the excitation energies only depend on ξ and F_2. Although the lowest excitation energies show good agreements (except for Tm with a little large error of ∼30%), we see disagreements overall. This is because the excitation energies are somehow sensitive to the small differences of ξ and F_2 in Table I.

Let us show our main results of Eu compounds, EuCl₃, EuN, and Eu-doped GaN. For Eu-doped GaN in the wurtzite structure, we use a 2×2×2 supercell (32 atoms per cell) substituting one Ga with Eu. We perform QSGW calculations for the crystal structure optimized by Quantum Espresso [50,51]. We show the QSGW results for EuCl₃ and EuN in the Supplemental Material [41]. In Table II, we show ξ, F_0, ΔF_0, F_2, and B_l^m. We see F_0 and ΔF_0 are strongly reduced from those of the free Eu ion. However, F_2 is not so different from that of free Eu ion. This finding suggests that F_2 given by Dieke is reasonable probably even in other solids. However, we see some complicated behavior of F_2 in detail: $F_2 = 0.058$ eV for the free Eu ion is reduced to be $F_2 = 0.053$ eV for EuN while a little enhanced to be $F_2 = 0.075$ eV for EuCl₃. On the other hand, $\xi = 0.195$ eV for free Eu ion is very different from $\xi = 0.093$ eV for Eu-doped GaN. Considering the expression of SOC, this is due to the delocalization of $4f$ orbitals in Eu-doped GaN, suggesting hybridization with other surrounding orbitals. The parameters for CF should be material dependent. In particular, we see that B_2^0 for the c-axis anisotropy is rather large (= 2.217 eV) for EuCl₃, while $B_2^0 = 0.346$ eV for Eu-doped GaN. Let us focus on Eu-doped GaN. As shown in Figs. 3(a) and 3(b), QSGW80 gives the band gap 3.78 (3.69) eV for the majority (minority) spin, corresponding to the experimental value of GaN 3.4 eV. Just above the bottom of the conduction band, we have an unoccupied band of $m = \pm3$ for the majority spin. In contrast to the unoccupied band, the occupied $4f$ orbitals are hybridized well with valence bands of GaN. Such hybridization is also seen in the calculations of the HSE functional [54]. In Fig. 3(c), we compare the eigenvalues of $\mathcal{H}_{HF}$ (blue lines) and those of

TABLE II. Parameters in eV determined by our method for Eu^{3+} in Eu compounds. See text for their definitions. For the calculations, we use crystal structures in references.

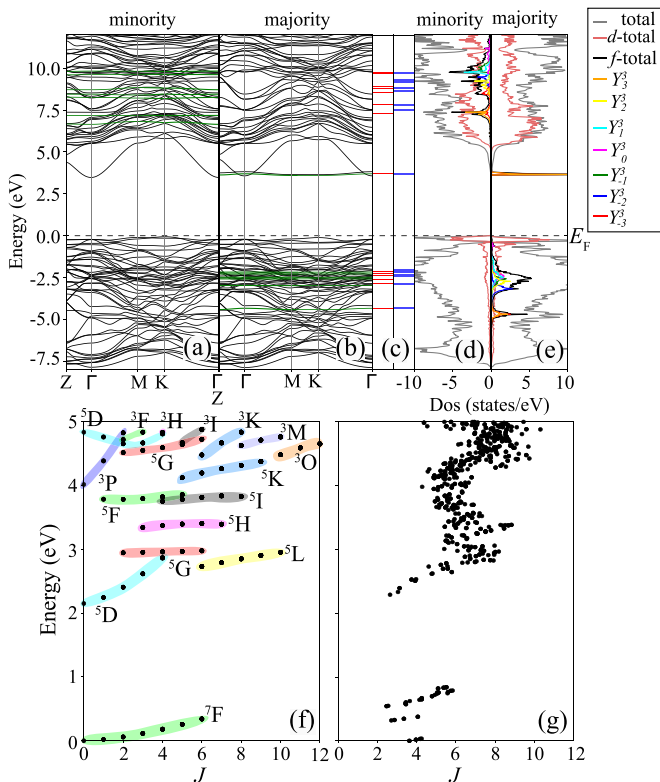| Material	ξ	F_0	ΔF_0	F_2	B_4^0	B_6^0	B_2^0	B_6^6
Free Eu ion (Table I)	0.195	14.803	0.481	0.058				
EuCl₃ [52]	0.203	8.773	0.340	0.075	0.017	0.004	2.217	−0.080
EuN [53]	0.156	5.565	0.150	0.053	0.000	−0.006		
Eu-doped GaN	0.093	6.703	−0.057	0.046	0.021	−0.002	0.346	−0.063

FIG. 3. [(a), (b)] The QSGW band structure of majority (minority) spin for Eu-doped GaN (black). We superpose band structure of $\mathcal{H}_{4f}^{\mathrm{QSGW}}$ (green). (c) Comparison of eigenvalues of $\mathcal{H}_{4f}^{\mathrm{QSGW}}$ (red) and those of $\mathcal{H}_{\mathrm{HF}}$ (blue). [(d), (e)] DOS and PDOS corresponding to the QSGW band structure. (f) The plot of eigenvalues of $\mathcal{H}$ for Eu-doped GaN classified by J neglecting $\mathcal{H}_{\mathrm{CF}}$. (g) The plot of eigenvalues of $\mathcal{H}$ for Eu-doped GaN classified by J.

$\mathcal{H}_{4f}^{\mathrm{QSGW}}$ (red lines). A little matching error indicates room for improving our method, while the error may not change our conclusions.

We show the eigenvalues of $\mathcal{H}$ in Fig. 3(g) obtained by the exact diagonalization. Here we classify the eigenvalues by the expectation values of total angular momentum J. In Fig. 3(f), we show eigenvalues when we neglect $\mathcal{H}_{\mathrm{CF}}$ in $\mathcal{H}$. Without $\mathcal{H}_{\mathrm{CF}}$, each eigenstate is represented by Russell-Saunders states. In Fig. 3(f) without CF, there is a large gap between ^7F and ^5D. The size of this gap is ~ 2 eV. This corresponds to the observed red emission, which is experimentally identified to be the transition from $^5D_0$ to $^7F_2$ [2]. Comparison of Figs. 3(f) and 3(g) shows that $\mathcal{H}_{\mathrm{CF}}$ is large enough to mix low-J and high-J eigenstates, resulting in a middle size of J. That is, $\mathcal{H}_{\mathrm{CF}}$ causes a sizable breaking of the Russell-Saunders coupling. However, $\mathcal{H}_{\mathrm{CF}}$ is not large enough to alter the overall structure. That is, we see remnants of ^5D and ^7F in Fig. 3(g) while the excitation gap between them is preserved. This justifies the use of the Dieke diagram for the analysis of PLR.

IV. CONCLUSION

In summary, we presented a new method to determine the model Hamiltonian from the QSGW calculations. By the exact diagonalization of the model Hamiltonian, we can justify the applicability of the Dieke diagram to RE in solids and its limitations. Along the line of our method, it is possible to include the hybridization of $4f$ electrons with others. In fact, our QSGW calculation shows we have large hybridization of occupied $4f$ orbitals with valence bands. We now have an extension of our method applied to multiplets of $3d$ orbitals working well [55].

[1] A. Steckl, J. Heikenfeld, D.-S. Lee, M. Garter, C. Baker, Y. Wang, and R. Jones, Rare-earth-doped GaN: growth, properties, and fabrication of electroluminescent devices, IEEE J. Sel. Top. Quantum Electron. **8**, 749 (2002).

[2] A. Nishikawa, N. Furukawa, T. Kawasaki, Y. Terai, and Y. Fujiwara, Improved luminescence properties of Eu-doped GaN light-emitting diodes grown by atmospheric-pressure organometallic vapor phase epitaxy, Appl. Phys. Lett. **97**, 051113 (2010).

[3] J. H. Park and A. J. Steckl, Laser action in Eu-doped GaN thin-film cavity at room temperature, Appl. Phys. Lett. **85**, 4588 (2004).

[4] J. C. Slater, The theory of complex spectra, Phys. Rev. **34**, 1293 (1929).

[5] G. Racah, Theory of complex spectra. IV, Phys. Rev. **76**, 1352 (1949).

[6] B. G. Wybourne, Structure of fn configurations. I. Calculation of the energy levels, J. Chem. Phys. **36**, 2295 (1962).

[7] G. S. Ofelt, Structure of the f^6 configuration with application to rare-earth-ions, J. Chem. Phys. **38**, 2171 (1963).

[8] W. T. Carnall, P. R. Fields, and K. Rajnak, Electronic energy levels in the trivalent lanthanide aquo ions. I. Pr^{3+}, Nd^{3+}, Pm^{3+}, Sm^{3+}, Dy^{3+}, Ho^{3+}, Er^{3+}, and Tm^{3+}, J. Chem. Phys. **49**, 4424 (1968).

[9] B. R. Judd, Optical absorption intensities of rare-earth ions, Phys. Rev. **127**, 750 (1962).

[10] G. S. Ofelt, Intensities of crystal spectra of rare-earth ions, J. Chem. Phys. **37**, 511 (1962).

[11] G. H. Dieke and H. M. Crosswhite, The spectra of the doubly and triply ionized rare earths, Appl. Opt. **2**, 675 (1963).

[12] P. E. M. Siegbahn, J. Almlöf, A. Heiberg, and B. O. Roos, The complete active space SCF (CASSCF) method in a Newton-Raphson formulation with application to the HNO molecule, J. Chem. Phys. **74**, 2384 (1981).

[13] L. Ungur and L. F. Chibotaru, *Ab initio* crystal field for lanthanides, Chem. Eur. J. **23**, 3708 (2017).

[14] L. Ungur, B. Szabo, Z. A. ALOthman, A. A. S. Al-Kahtani, and L. F. Chibotaru, Mechanisms of luminescence in lanthanide complexes: A crucial role of metal-ligand covalency, Inorg. Chem. **61**, 5972 (2022).

[15] F. Steglich, J. Aarts, C. D. Bredl, W. Lieke, D. Meschede, W. Franz, and H. Schäfer, Superconductivity in the Presence of Strong Pauli Paramagnetism: CeCu$_2$Si$_2$, Phys. Rev. Lett. **43**, 1892 (1979).

[16] Z. Wu, Y. Fang, H. Su, W. Xie, P. Li, Y. Wu, Y. Huang, D. Shen, B. Thiagarajan, J. Adell, C. Cao, H. Yuan, F. Steglich, and Y. Liu, Revealing the Heavy Quasiparticles in the Heavy-Fermion Superconductor CeCu$_2$Si$_2$, Phys. Rev. Lett. **127**, 067002 (2021).

[17] S. Patil, A. Generalov, M. Güttler, P. Kushwaha, A. Chikina, K. Kummer, T. C. Rödel, A. F. Santander-Syro, N. Caroca-Canales, C. Geibel *et al.*, ARPES view on surface and bulk hybridization phenomena in the antiferromagnetic Kondo lattice CeRh$_2$Si$_2$, Nat. Commun. **7**, 11029 (2016).

[18] D. V. Vyalikh, S. Danzenbächer, Y. Kucherenko, K. Kummer, C. Krellner, C. Geibel, M. G. Holder, T. K. Kim, C. Laubschat, M. Shi, L. Patthey, R. Follath, and S. L. Molodtsov, k Dependence of the Crystal-Field Splittings of 4f States in Rare-Earth Systems, Phys. Rev. Lett. **105**, 237601 (2010).

[19] J. Hubbard and B. H. Flowers, Electron correlations in narrow energy bands, Proc. R. Soc. A. Math. Phys. Sci. **276**, 238 (1963).

[20] A. I. Lichtenstein and M. I. Katsnelson, *Ab initio* calculations of quasiparticle band structure in correlated systems: LDA++ approach, Phys. Rev. B **57**, 6884 (1998).

[21] A. Svane, V. Kanchana, G. Vaitheeswaran, G. Santi, W. M. Temmerman, Z. Szotek, P. Strange, and L. Petit, Electronic structure of samarium monopnictides and monochalcogenides, Phys. Rev. B **71**, 045119 (2005).

[22] S. Lebègue, G. Santi, A. Svane, O. Bengone, M. I. Katsnelson, A. I. Lichtenstein, and O. Eriksson, Electronic structure and spectroscopic properties of thulium monochalcogenides, Phys. Rev. B **72**, 245102 (2005).

[23] S. Lebègue, A. Svane, M. I. Katsnelson, A. I. Lichtenstein, and O. Eriksson, Multiplet effects in the electronic structure of light rare-earth metals, Phys. Rev. B **74**, 045114 (2006).

[24] C. H. Kim, S. Baidya, H. Cho, V. V. Gapontsev, S. V. Streltsov, D. I. Khomskii, J.-G. Park, A. Go, and H. Jin, Theoretical evidence of spin-orbital-entangled $J_{eff} = \frac{1}{2}$ state in the 3d transition metal oxide CuAl$_2$O$_4$, Phys. Rev. B **100**, 161104(R) (2019).

[25] Y. Lee, T. Kotani, and L. Ke, Role of nonlocality in exchange correlation for magnetic two-dimensional van der Waals materials, Phys. Rev. B **101**, 241409(R) (2020).

[26] T. Kotani, M. van Schilfgaarde, and S. V. Faleev, Quasiparticle self-consistent GW method: A basis for the independent-particle approximation, Phys. Rev. B **76**, 165106 (2007).

[27] D. Deguchi, K. Sato, H. Kino, and T. Kotani, Accurate energy bands calculated by the hybrid quasiparticle self-consistent GW method implemented in the ecalj package, Jpn. J. Appl. Phys. **55**, 051201 (2016).

[28] A. N. Chantis, M. van Schilfgaarde, and T. Kotani, Quasiparticle self-consistent GW method applied to localized 4f electron systems, Phys. Rev. B **76**, 165126 (2007).

[29] H. Okumura, K. Sato, and T. Kotani, Nonlinear extension of the dynamical linear response of spin: Extended Heisenberg model, J. Phys. Soc. Jpn. **90**, 094710 (2021).

[30] J. A. Gaunt and R. H. Fowler, IV. The triplets of helium, Philos. Trans. R. Soc. London A **228**, 151 (1929).

[31] E. U. Condon and G. H. Shortley, The theory of complex spectra II, Phys. Rev. **37**, 1025 (1931).

[32] E. Trefftz, Theoretische Ansätze zur Deutung des Pr IV-Spektrums, Z. Phys. **130**, 561 (1951).

[33] B. R. Judd and M. H. L. Pryce, The theory of the spectra of europium salts, Proc. R. Soc. A. Math. Phys. Sci. **228**, 120 (1955).

[34] K. W. H. Stevens, Matrix elements and operator equivalents connected with the magnetic properties of rare earth ions, Proc. Phys. Soc. A **65**, 209 (1952).

[35] ecalj package is available from https://github.com/tkotani/ecalj/.

[36] H. Sakakibara, T. Kotani, M. Obata, and T. Oda, Finite electric-field approach to evaluate the vertex correction for the screened Coulomb interaction in the quasiparticle self-consistent GW method, Phys. Rev. B **101**, 205120 (2020).

[37] H. Sakakibara, S. W. Jang, H. Kino, M. J. Han, K. Kuroki, and T. Kotani, Model-mapped RPA for determining the effective Coulomb interaction, J. Phys. Soc. Jpn. **86**, 044714 (2017).

[38] A. N. Chantis, M. van Schilfgaarde, and T. Kotani, *Ab Initio* Prediction of Conduction Band Spin Splitting in Zinc Blende Semiconductors, Phys. Rev. Lett. **96**, 086405 (2006).

[39] N. Marzari and D. Vanderbilt, Maximally localized generalized Wannier functions for composite energy bands, Phys. Rev. B **56**, 12847 (1997).

[40] We placed our original code of this calculation on github as https://github.com/ktszk/eigloc.

[41] See Supplemental Material at http://link.aps.org/supplemental/10.1103/PhysRevResearch.5.013111 for QSGW results of free RE^{+3} ions except for Eu^{+3}, and QSGW results of EuCl$_3$ and EuN.

[42] R. J. Lang, The spectrum of trebly ionized cerium, Can. J. Res. **13a**, 1 (1935).

[43] R. J. Lang, The spectrum of trebly ionized cerium, Can. J. Res. **14a**, 127 (1936).

[44] B. R. Judd and B. Bleaney, An analysis of the fluorescence spectrum of neodymium chloride, Proc. R. Soc. A. Math. Phys. Sci. **251**, 134 (1959).

[45] J. B. Gruber and J. G. Conway, Crystal field splitting of energy levels of thulium ethylsulfate, J. Chem. Phys. **32**, 1531 (1960).

[46] W. A. Runciman, Analysis of the spectra of gadolinium salts, J. Chem. Phys. **30**, 1632 (1959).

[47] J. S. Margolis, Energy levels of PrCl$_3$, J. Chem. Phys. **35**, 1367 (1961).

[48] M. H. Crozier and W. A. Runciman, Analysis of the spectra of trivalent promethium and holmium, J. Chem. Phys. **35**, 1392 (1961).

[49] F. Varsanyi and G. H. Dieke, Energy levels of hexagonal ErCl$_3$, J. Chem. Phys. **36**, 2951 (1962).

[50] P. Giannozzi, S. Baroni, N. Bonini, M. Calandra, R. Car, C. Cavazzoni, D. Ceresoli, G. L. Chiarotti, M. Cococcioni, I. Dabo *et al.*, QUANTUM ESPRESSO: A modular and open-source software project for quantum

simulations of materials, J. Phys.: Condens. Matter **21**, 395502 (2009).

[51] We use the wave functions expanded by plane waves up to cut-off energy of 60.0 Ry and 8^3 k-point mesh for optimization.

[52] K. Persson, Materials data on $EuCl_3$ (SG:176) by Materials Project (2016), doi: 10.17188/1275324.

[53] P. Larson, W. R. L. Lambrecht, A. Chantis, and M. van Schilfgaarde, Electronic structure of rare-earth nitrides using the LSDA+U approach: Importance of allowing $4f$ orbitals to

break the cubic crystal symmetry, Phys. Rev. B **75**, 045114 (2007).

[54] K. Hoang, Rare-earth defects in GaN: A systematic investigation of the lanthanide series, Phys. Rev. Mater. **6**, 044601 (2022).

[55] H. Saito, K. Suzuki, K. Sato, and T. Kotani, Construction of model Hamiltonians for the transition-metal impurities via the QSGW method, Research Square, doi: 10.21203/rs.3.rs-2563338/v1.